Received: August 15, 2022. Revised: September 13, 2022. 443

International Journal of
Intelligent Engineering & Systems

http://www.inass.org/

Design of a Two-Area Automatic Generation Control Using a Single Input Fuzzy Gain Scheduling PID Controller

Mohammed Kh. Al-Nussairi[1]* Sadeq D. Al-Majidi[1] Ali Jber Mshkil[1]
Adel Manaa Dakhil[1] Maysam F. Abbodm[2] Hamed S. Al-Raweshidy[2]

[1]Department of Electrical Engineering, College of Engineering, University of Misan, Amarah 62001, Iraq
[2]Department of Electronic and Computer Engineering, College of Engineering, Design and Physical Sciences, Brunel University London, Uxbridge UB8 3PH, United Kingdom
* Corresponding author's Email: muhammed.kh@uomisan.edu.iq

Abstract: An Automatic Generation Control (AGC) is considered a substantial stage in power systems to ensure that the area-frequency response and the tie-line power of an interchanging steady state errors are acceptable values especially at the transient state. Whiles, several techniques have been designed for the AGC, Fuzzy logic control is commonly used. However, it is faced a longer processing time issues to adjust the accurate single in the transient state. In this paper, a Single Input Fuzzy Logic Gain Scheduling PID Controller (SIFL-PID) is designed as a supplementary loop for AGC of two area interconnected power system to reduce the processing time. The lower number of rules and the simple parameters of the SIFL-PID will contribute to minimise the design time required for the Fuzzy Logic Gain Scheduling FL-PID. The SIFL-PID also reduced the signed distance technique when it is generated one input variable simple mathematical model of the system. In comparison with the FL-PID, the number of rules controlling system can be significantly reduced. The main outcome of this work is that it is assessed the effectiveness of the SIFL-PID for two power systems that are interconnected when it is compared with the FL-PID using the MATLAB/SIMULINK environment. The results prove that, the simple design of the SIFL-PID control is validated under various condition tests. Performance analysis standards are also performed. The results of all simulations demonstrate that the suggested controller provides better performances such as like as minimum Performance analysis standards, frequency deviation power deviations and low overshoot and undershoot.

Keywords: Two area interconnected power system, Automatic generation control, PID controller, Fuzzy gain scheduling PID controller, Single input fuzzy logic, Frequency deviations.

1. Introduction

A concept of a power system is that the interconnection of a large number of control areas are connected to one another, and these control areas comprise coherent groupings of generators [1]. Tie lines are used to connect the control areas to one another. The interconnection of power systems is necessary in order to maintain the efficient flow of power supply and to improve the system's level of reliability [2, 3]. Each area contains own generation unit and is supply of its own load-demand and scheduled exchanges with neighbouring areas. Because the load on a particular power system is always changing, the system frequency and tie-line power flows will depart from the nominal values that were designed for each. Automatic generation control, often known as AGC, is a component that must be present for the operation of an electric power system to be considered stable [4].

AGC is an important control system that runs continuously in interconnected power systems to maintain a balance between the load and the generation at the lowest possible cost. The AGC systems have the advantage of adjusting the frequency, managing the exchange of power, and providing economic dispatch. The AGC process gives about the necessary adjustments in generation by transmitting signals to the generating units that are

under its control. The operation of AGC is particularly dependent on the approach in which those generating units respond to the commands. The response parameters of the generator unit are sensitive to a wide variety of factors, including the type of unit, the fuel, the control strategy, and the operating point [3-5].

Frequency deviation is a useful metric for deciding the load-demand with the power generation by the connected generation unit are already out of balance. An off-normal frequency deviation that is persistent has a direct impact on the functioning of the power system, as well as its reliability, security, and overall efficiency. This occurs because the deviation causes equipment damage, overloads transmission lines, decreases load performance, and engages protection devices [2, 6].

There are two main control loops in the AGC scheme. These control loops are referred to as primary and secondary, respectively. The primary loop control, is responsible for achieving the main objective of real power balance by modifying the output of the turbine to meet a change in the demand placed on it by the load. The change in the generation is a result of contributions from all of the participating generating units. However, steady-state frequency deviations are produced whenever there is a change in the load. In order to return the frequency to its nominal value, an additional control loop, which is referred to as the secondary loop or supplementary loop, is required. The use of one of the Control Techniques that reduce frequency deviations to levels that are considered suitable allows for the successful completion of this purpose [2].

Hence, several control mechanisms have been suggested for the power systems' AGC. In this regard, many AGC control strategies are put out in the literature [1, 2, 4, 7] and are categorized into three groups. The first group of controllers is known as Conventional Control Techniques, which are including; Linear-Quadratic-Regulator-Based Controlling Technique [8], and Proportional-Integral-Derivative (PID) Controlling-Technique [9]. PI and PID control structures have found widespread use in power system control because of their low cost and easy implementation. In real AGC applications, knowledgeable human experts typically carry out tuning the PI and PID gains; consequently, it may be impossible to achieve a performance level that is desirable for AGC in large-scale power systems that have a high order nonlinearities, time delays, and uncertainties in the absence of precise mathematical models [1].

The second group includes Model predictive controls[10], adaptive and sliding mode controls [11], optimal controls, which are known as modern controls. However, in order to remain effective, these control strategies require some previous knowledge of the system states, which are not always simple to determine in their totality [1].

The third group is Modern Soft Computing Techniques, which are mostly based on fuzzy logic control. Fuzzy logic is utilized in practically every area of science and technology today due to its ease of use, robustness, and reliability [2]. One example of this is the employment of fuzzy logic to solve a wide variety of control challenges in the operation and control of power systems. In contrast, it is efforts to establish the controller in a way that is directly dependent on the measurements, knowledge of the domain experts and operators, and long-term experiences due to a fundamentally linearized mathematical model [12]. In comparison to the PI controller, which may implement a well-established design procedure such as the bode-plot methodology and the Nyquist method, there is currently no standardized method for the design of FLCs. As a result, stability and optimal performance are sometimes challenging to accomplish[13, 14].

This one has recently come to widespread attention that combining fuzzy logic with PID controller is an effective way to improve the AGC system's overall performance by taking full advantage of both control strategies [15, 16]. An efficient solution to the issue of PID parameters online self-tuning can be achieved through the utilization of a fuzzy logic gain scheduling. It makes it possible for the fuzzy rule base to take action on the parameters of the PID controller and to change these parameters in real time according to the error and its derivative[17]. Because of this, the PID controller may very well be adjusted to non-linear systems as well as all of the operating conditions of the system.

Typically, the conventional fuzzy logic (CFL) is implemented with two input sensors; an error and change of error. In addition, processes of fuzzification and defuzzification, as well as an inference mechanism and storage for rule bases build the structure of fuzzy logic control. Because of these features, the controller will naturally become more complicated, which will require a significant amount of additional computing time [18-21]. However, these research does not discuss the issue of tuning FLC which is considered the major challenge to design accurate controller. Consequently, it is possible that those methods are not suitable for implementation in real-time with a small sample time as is needed in AGC [13].

In this paper, the design of AGC for two area interconnected power system with Single Input

Fuzzy Gain Scheduling PID Controller (SFLC-PID) is proposed. Conventional fuzzy logic is the basis for the formation of single-input fuzzy logic that has been introduced by [22]. Instead of using two variables as inputs like fuzzy logic does, the SIFLC just uses one variable for its computation [23, 24]. Because it only require one input variable, single-input fuzzy logic controllers (SIFLC) provide less of a computational burden on the digital processor than CFLC [25]. It brings the two-dimensional Toeplitz rule base down to a one-dimensional rule vector, which can be approximated using a piecewise linear control surface. According to the results of computer simulations, the control performance is almost similar to that of a conventional fuzzy logic controller [18, 26].

A MATLAB/ simulation of two areas of interconnected power is proposed to test the corresponding PID controller, a conventional Fuzzy Gain Scheduling PID Controller, and a Single Input Fuzzy Gain Scheduling PID Controller. This paper is organized as following: The interconnected power system model of AGC for two areas is discussed in Section 2, The complete description of PID, FL-PID, and SIFL-PID controller structures is introduced in Section 3, while Section 4 includes the simulation results. Finally, Section 5 reports the conclusion.

2. Two area interconnected power system

2.1 Modelling of two area interconnected power system

The term "two-area interconnected power system" consists of a system that has tie line connected with the two control areas. In this power system, each area provides power to its own area, and the tie line is responsible for facilitating the flow of power between areas. Each area of the Two Area Interconnected Power System represents the turbine, governor, synchronous generator (mass rotating), and load models all in one compact system. One of the most typical methods employed in mathematical modelling of this system for the purpose of control system analysis and design is widely recognized as the transfer function as shown in the Fig. 1.

It is possible to obtain the model of the generator unit by first using the swing equation based on a thin incremental change. Next, the Laplace transform is taken as given in Eq. (1) [27]:

$$\Delta\Omega(s) = \frac{1}{2Hs}(\Delta P_m - \Delta P_e) \tag{1}$$

where $\Omega(s)$ is represented the generation speed, H is represented the generation inertia, ΔPm is represented the variation of the mechanical power, and ΔPe is represented the variation of the electrical power.

The load can be broken down into two categories: the first category has an independent-frequency, such as a resistive load, while the second category is sensitive-load to frequency- deviation included motors.

$$\Delta P_e = \Delta P_L + D\Delta\omega \tag{2}$$

where the $D\Delta\omega$ is the sensitive-load and the P_L is constant sensitive load.

Finally, A gain K and a time constant $\boldsymbol{\tau}_P$ are used to represent the generator (the rotating mass) and the load, as given by:

$$\frac{\Delta\Omega}{\Delta P_m(s) - \Delta P_e(s)} = \frac{K}{1+\tau_P s} \tag{3}$$

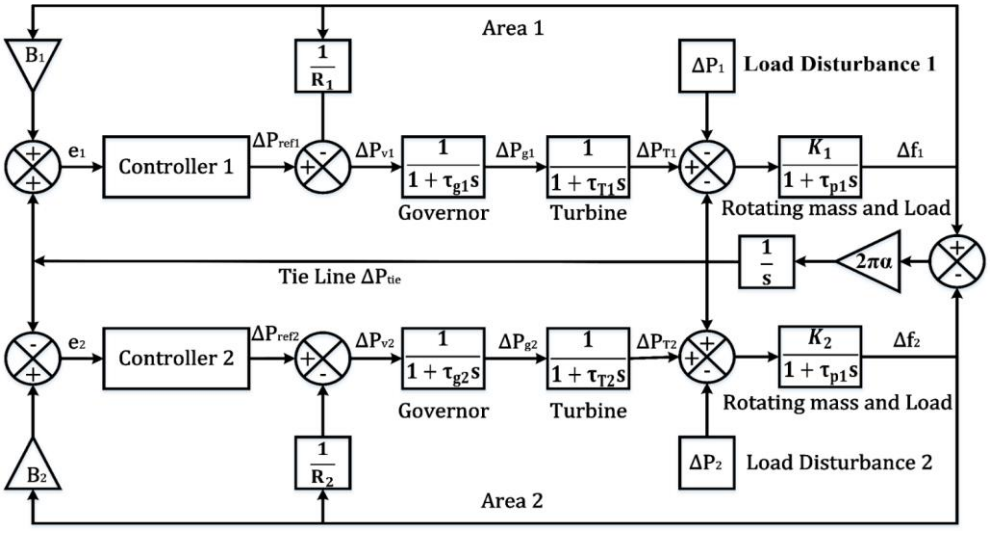

Figure. 1 AGC block diagram of a two area interconnected power system

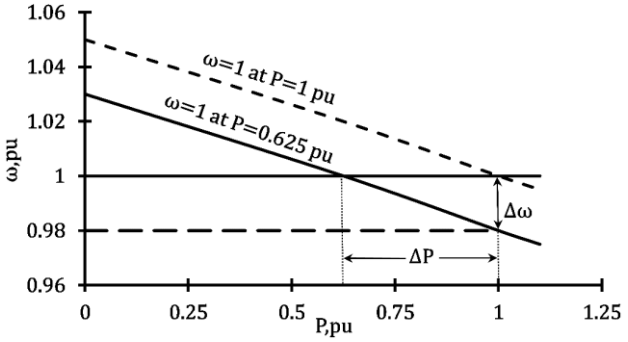

Figure. 2 Steady state speed characteristics of governor

The mechanical power that is produced by the turbine is proportional to the adjustments made to the steam valve position as given by

$$\frac{\Delta P_m(s)}{\Delta P_v(s)} = \frac{1}{1+\tau_T s} \tag{4}$$

Where τ_T is represented the time constant of standard speed turbine. The essential duty of a speed governor in a turbine is to modify the output power P_g by making adjustments depending on the values of the reference power P_{ref} and the power $\Delta\Omega/R$ of the system.

$$\Delta P_g = \Delta P_{ref} - \frac{\Delta\Omega(s)}{R} \tag{5}$$

where R denotes the adjustable speed regulator. As seen in Fig.4, the speed of rotation of the turbine slows down when there is an increase in the connected load. It is possible to suppose that it has a linear relationship with the time constant $\boldsymbol{\tau}_g$, as given transfer function:

$$\frac{\Delta P_v}{\Delta P_g} = \frac{1}{1+\tau_g} \tag{6}$$

Fig. 2 shows the one control area has three inputs that are refer as load disturbance ΔP, tie line power ΔP_{tie} and the power reference ΔP_{ref}. the area control area e error and frequency error Δf is represented the output of these system. The area control area e is given by:

$$e = -B\Delta f \mp \Delta P_{tie} \tag{7}$$

$$B = \frac{1}{R} + D \tag{8}$$

2.2 Tie line power flow

A two-area power system is represented by two generating units which are connected by a less tie line with Xtie-reactance. As can be seen in Fig. 3, each

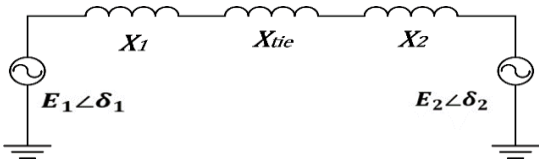

Figure. 3 Two area power system equivalent circuit

area is characterized by a voltage source that is followed by an equivalent reactance.

Eq. (9) is used to determine the active power transferred through the tie line in normal operating conditions.

$$P_{12} = \frac{|E_1||E_2|}{X_{12}} \sin\delta_{12} \tag{9}$$

where

$$X_{12} = X_1 + X_2 + X_{tie} \tag{10}$$

And

$$\delta_{12} = \delta_1 - \delta_2 \tag{11}$$

If a small change occurs in the rotor angle, δ; then the resultant power on the tie line, ΔP_{12}, can be calculated by using Eq. (12).

$$\Delta P_{12} = \frac{dP_{12}}{d\delta_{12}}\Big|_{\delta_{12}} \Delta\delta_{12} = P_s \Delta\delta_{12} \tag{12}$$

P_s is the synchronizing power coefficient, which is define as the slope of the power angle curve at beginning operating angle $\Delta\delta_{12}=\Delta\delta_1-\Delta\delta_2$. Ps can be determined by given eq

$$P_s = \frac{dP_{12}}{d\delta_{12}}\Big|_{\delta_{12}} = \frac{|E_1||E_2|}{X_{12}} \cos\delta_{12} \tag{13}$$

The tie-line power deviation can be written into its final form

$$\Delta P_{12} = P_s\, \Delta\delta_{12} \tag{14}$$

Depending on the direction the power flow, the tie-line power flow may present as an increase in load in one region while simultaneously causing a decrease in load in another area, i.e, if $\delta_1>\delta_2$ then the power is transmitted from area 1 to area 2.

Assuming a change in the load in area 1, denoted by ΔP_1, at the time when the frequency was at its steady state i.e $\Delta f=\Delta f_1=\Delta f_2$, and for first area

$$P_{m1} - \Delta P_{m2} - \Delta P_{12} = \Delta f D_1 \tag{15}$$

And for Second area:

$$\Delta P_{m2} + \Delta P_{12} = \Delta f D_2 \tag{16}$$

Using the governor speed characteristic, it is determined that mechanical power changes and is given as:

$$\Delta f = \frac{-\Delta P_1}{B_1+B_2} \quad (17)$$

$$\Delta P_{12} = \frac{-\Delta P_1 B_1}{B_1+B_2} \quad (18)$$

When the load in area1 goes up by ΔP_1, the frequency decreases in both areas and a tie-line power flow of ΔP_{12} occurs. When the ΔP_{12} is positive, flow is occurring from area 1 to area 2, and when it is negative, flow is occurring in the other direction, from area 2 to area 1.

The deviation of the tie line is a reflection of the contribution of the regulation that is characteristic of one area to another. The main goal of supplementary control is that it is re-establishes the equilibrium between the load generations in all of the different areas. This goal is accomplished when the control action is capable of maintaining: Frequency should be kept close to the nominal value, as much as possible, keep the flow of the tie line roughly on schedule at all times. Hance, each area will be able to absorb the changes in its own load.

In an ideal situation, the supplementary control should just adjust for changes in that specific area. In other words, if something changes in area 1, then the supplemental control should only apply to Area 1 and not in area 2. In order to accomplish this goal, the area control error is applied which is given by

For area-1

$$e_1 = \Delta P_{12} + B_1 \Delta f \quad (19)$$

For area-2

$$e_2 = \Delta P_{21} + B_2 \Delta f \quad (20)$$

The deviation of tie-line power flowing in between adjacent control areas during transient events is commonly denoted ΔP_{tie}. This value is obtained by:

$$\Delta P_{tie} = \frac{2\pi\alpha}{s}(\Delta f_1 - \Delta f_2) \quad (21)$$

3. Controller structure

3.1 PID controller

The PID control structure is composed of the addition of three different components, which are referred to as the proportional, integral and derivative of error value, respectively. Therefore, the PID controller's indicated transfer function can be written as follows:

$$u(t) = K_p e(t) + K_i \int_0^t e(t)dt + K_d \frac{de(t)}{dt} \quad (22)$$

The constant values of major PID parameters Kp , K_i and K_d correspond to the proportional, integral and derivative, respectively. The controller is applied to improve the dynamic performance; the main aim of this is to adjust the error value at stability state. The dynamic response can be made more stable with the use of proportional constants by reacting to changes that take place in the observed error value. The integral inserts a pole at the origin increases system type by one and eliminates step function steady-state error. The derivative provides an open loop system, with a finite zero, which improves the system's response to transient conditions.

PID tuning refers to the process of setting controller parameters in order to meet a set of predefined performance targets. There are two main classifications that can be used to classify the PID controllers that are discussed in the relevant literature. The controller parameters in the first category are fixed during control processing after they have been tweaked or chosen in an optimal manner. Second category controllers are built in a manner similar to PID controllers. However, their parameters are modified online based on parameter estimation, which requires particular knowledge of the system, such as the structure of the system model. This knowledge is required in order for the parameter estimate to be performed. The use of knowledge-based systems in the control of processes is becoming widespread, particularly in the topic of fuzzy logic. In fuzzy logic, the linguistic representations of human expertise in controlling the system are described as fuzzy inference or relationships. This provides more flexibility in the controller design.

3.2 Fuzzy gain scheduling PID controller

In the description of the Fuzzy-PID controller, there are the major value of PID controller; K_p , K_i, and K_d which are tuned based on Fuzzy Logic (FL) as depicted in Fig. 4 . It is often difficult to tune the K_p, K_i and K_d of the PID controller for a system that has a high degree of nonlinearity with uncertain parameter changes. This is because that the system's behaviour can be unpredictable. Consequently, the process of tuning the PID parameters ought to have been done in an automated manner. Fig. 4 depicts the overall architecture of the Fuzzy-PID controller.

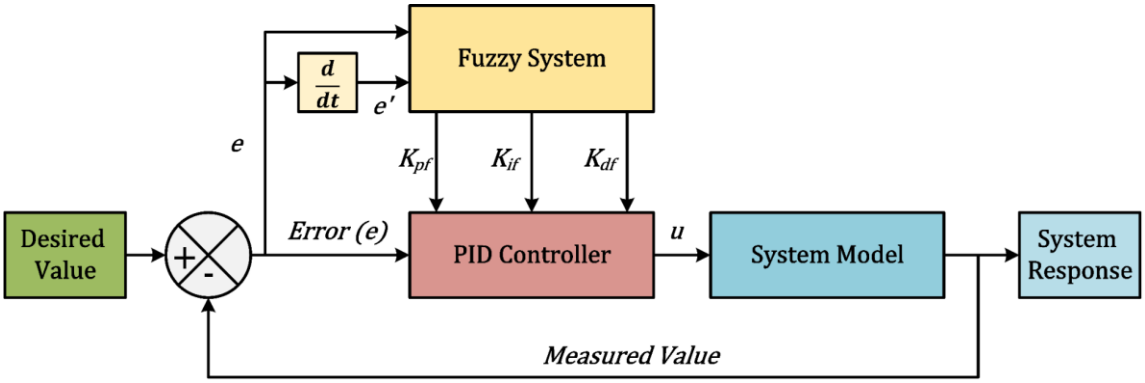

Figure. 4 Fuzzy gain scheduling PID controller scheme

The fuzzy logic, which generates a nonlinear scaling from the error and derivative of error to the PID parameter values, is used to tune the coefficients of the PID transfer function, which results in PID values that are more accurate. The scheme of the fuzzy logic block shown in Fig. 5 has two inputs, which are designated as error e(t) and derivative e'(t), and it has three outputs, which are referred to as K_{pf}, K_{if} and K_{df} respectively. According to Eq. (23), K_{pf}, K_{if} and K_{df} are added to K_p , K_i and K_d correspondingly. The values of K_{pf}, K_{if} and K_{df} are derived from the fuzzy logic block, and their values dynamically and continually adjust in response to the changing operating conditions of the interconnected power system.

The scheme of the fuzzy logic block shown in Fig. 4 has two inputs, which are designated as error e(t) and derivative e'(t), and it has three outputs, which are referred to as K_{pf}, K_{if} and K_{df} respectively. According to Eq. (23), K_{pf}, K_{if} and K_{df} are added to K_p , K_i and K_d correspondingly. The values of K_{pf}, K_{if} and K_{df} are derived from the fuzzy logic block, and their values dynamically and continually adjust in response to the changing operating conditions of the interconnected power system.

$$u(t) = \left(K_p + K_{pf}\right)e(t) + \left(K_i + K_{if}\right) \int_0^t e(t)dt + \left(K_d + K_{df}\right)\frac{de(t)}{dt} \quad (23)$$

The Mamdani model is applied as the structure of the fuzzy logic; however, several improvements have been made in order to achieve accurate values for K_{pf}, K_{if} and K_{df}. Following the application of the seven membership functions to frequency deviations and its derivative accordingly, the total number of rules is estimated to be 49. The membership function can be divided into 7 different groups, which are labelled as follows: ZE: Zero, NB: Negative Big, NM: Negative Medium, NS: Negative Small, PS: Positive Small, PM: Positive Medium, and PB: Positive Big.

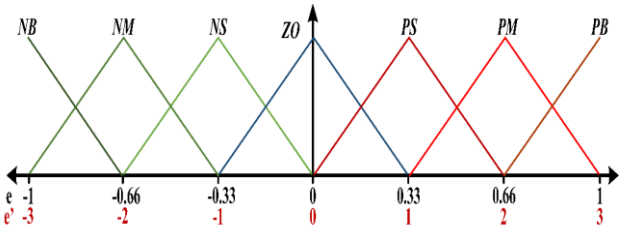

Figure. 5 Memberships of e and e'

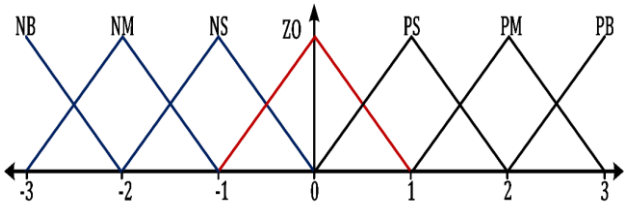

Figure. 6 Memberships of K_{pf}, K_{if} and K_{df}

Analysis of the time-domain system response curve seen in Fig. 5 is used to build the rule base table. The positive error extreme points are represented by the symbols that are indicated in Fig. 5 (including the symbols a, e, and i). The symbols that are being highlighted in Fig. 5 indicates the positive value extreme points (such as a, e and i), the negative value extreme points (such as C and G), and the zero value points (such as b, d, f and h). Fig. 5 shows a response curve that is composed of four different sorts of sections, which can be characterized as follows[16].

The frequency deviation varies from the point of extreme positive error to the point when it is been close to zero-error (like as ab and ef). It is necessary to increase k_p and k_i while decreasing k_d in order to make the necessary adjustments to the PID parameters so that the response speed can be improved close to the point of excessive positive error. Nevertheless, k_p and k_i are lowered, and k_d is raised in order to enhance the amount of overshoot

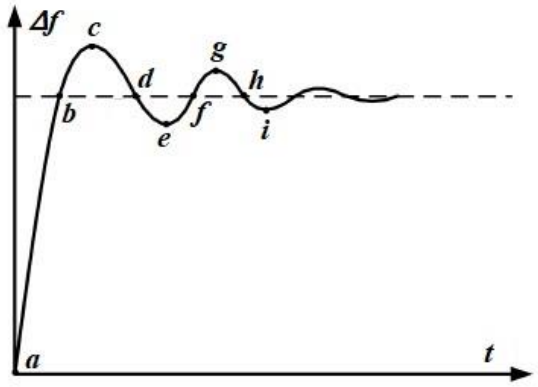

Figure. 7 The response curve of a system

Table 1. The rule table for K_{pf}

é \ e	NB	NM	NS	ZO	PS	PM	PB
NB	PB	PB	PB	PB	PM	PS	ZO
NM	PB	PB	PB	PM	PS	ZO	PS
NS	PB	PB	PM	PS	ZO	PS	PM
ZO	PB	PM	PS	ZO	PS	PM	PB
PS	PM	PS	ZO	PS	PM	PB	PB
PM	PS	ZO	PS	PM	PB	PB	PB
PB	ZO	PS	PM	PB	PB	PB	PB

Table 2. The rule table for K_{if}

é \ e	NB	NM	NS	ZO	PS	PM	PB
NB	NB	NB	NB	NB	NB	NM	ZO
NM	NB	NB	NB	NB	NM	ZO	PS
NS	NB	NB	NB	NM	ZO	PS	PM
ZO	NB	NB	NM	ZO	PS	PM	PB
PS	NB	NM	ZO	PS	PM	PB	PB
PM	PS	ZO	PS	PM	PB	PB	PB
PB	ZO	PS	PM	PB	PB	PB	PB

Table 3. The rule table for K_{df}

é \ e	NB	NM	NS	ZO	PS	PM	PB
NB	PB	PB	PB	PB	PM	PS	ZO
NM	PB	PB	PB	PM	PS	ZO	NS
NS	PB	PB	PM	PS	ZO	NS	NM
ZO	PB	PM	PS	ZO	NS	NM	PB
PS	PM	PS	ZO	NS	NM	PB	PB
PM	PS	ZO	NS	NM	PB	PB	PB
PB	ZO	NS	NM	PB	PB	PB	PB

that can be suppressed when the output frequency deviations are getting closer to the zero-error point.

The frequency deviations move away from the zero-error point and toward the extreme point of negative error (such as bc and fg). At this stage of the process, one of the objectives for regulating the PID coefficients is to reduce the effects of the overshoot by increasing k_p and k_d while decreasing k_i.

After reaching an extreme point of negative error, the frequency deviations move toward the point of zero-error (such as cd and gh). the regulation of the PID parameters in this segment is dictated by the upper right part of the rule table. This results in an undesirable rapid response speed near the zero-error point. The undesirable rapid response time would result in an increase in the undershoot, which, thankfully, would be reduced in the subsequent segment.

The frequency variation changes from the zero-value to the positive value (such as de and hi). In this section, the PID coefficients are adjusted to minimise the magnitude of the overshoot by raising the parameter of PID controller. The modifications that will need to be performed to the PID constants in different sections of the curve-response are detailed in Table 1 to 3.

3.3 Single input fuzzy logic (SIFL)

In Conventional Fuzzy Logic (CFL), the input contains the error and the variation of this error while the output contains form a two-dimensional rule. Table 1 to 3 show the rules table structure of a typical Toeplitz CFL. These tables have the Toeplitz array's diagonal output membership. Moreover, the magnitude of each point along a particular diagonal line is proportional to its distance from its main diagonal line.

As noticed from those Tables, a consistent pattern in the output memberships allows for even more simplification. Instead of utilizing two variables, a single variable can be used to generate the desired result. This single variable input represents the absolute distance (d) between a parallel line and the main diagonal line L_Z. To calculate the distance (d), let A be an intersection point on the main diagonal line and the line vertical to it from a known operation point B, as depicted in Fig. 6. The main diagonal line is derived as follows.

$$s: e + \lambda \dot{e} = 0 \tag{24}$$

The absolute distance between points A and B is given as follows [24]. A and B's distance can be calculated as

$$d_1 = \sqrt{(e_0 - e_1)^2 + (\dot{e_0} - \dot{e_1})^2} = \frac{|\dot{e_1} + \lambda e_1|}{\sqrt{1+\lambda^2}} \tag{25}$$

As indicated from Fig. 6, the λ is presented the slope of the main diagonal line LZ. The following equation is a generalization of Eq. (25):

$$d = \frac{|\dot{e} + \lambda e|}{\sqrt{1+\lambda^2}} \tag{26}$$

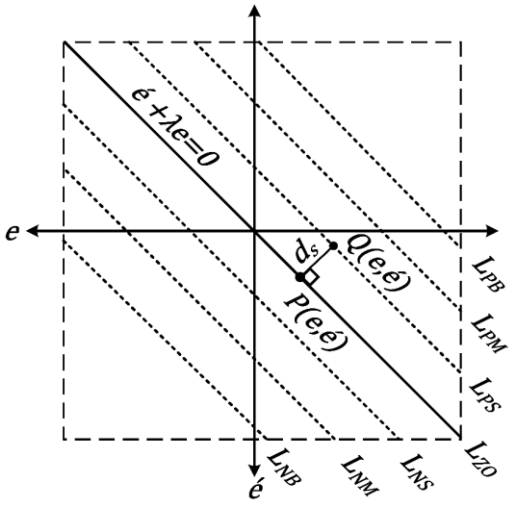

Figure. 8 Derivation of d_s

While the signed distance for any arbitrary point A is defined as:

$$d_s = sgn(s)\frac{|e^{\cdot}+\lambda e|}{\sqrt{1+\lambda^2}} = \frac{e^{\cdot}+\lambda e}{\sqrt{1+\lambda^2}} \quad (27)$$

where

$$sgn(s) = \begin{cases} 1 & for\ s > 0 \\ -1 & for\ s < 0 \end{cases} \quad (28)$$

Since the sign of the control, input is negative when s is less than 0 and positive when s is greater than 0, and its magnitude is proportional to the distance from 0, we can deduce that:

$$u \propto -d_S \quad (29)$$

As a result, the entire control action is obtained solely from ds. Next, the SIFL is referred. The resulting distance ds can convert the two-side rule table into a one-side rule, as illustrated in Table 4. Where the main side lines are denoted as L_{PL}, L_{PM}, L_{PS}, L_{ZO}, L_{NS}, L_{NM}, and L_{NB} respectively. These side represent input, and the output of the diagonal line that corresponds to them may be observed in Table 4.

Fig. 7 depicts the SIFL's structure, the signed dimension was used to obtain this structure. Control output u changes as a result of the fuzzy logic's input d. CFL and SIFL can be differentiated from one another. The input and output membership functions of the CFL is presented in Fig. 6. In comparison to CFL, the biggest benefit of SIFL is the reduction of rules. For a typical CFL with two inputs and a fuzzification level of n, the number of rules to infer is n^2. In contrast, SIFL simply requires n rules. According to the approach stated in [24, 25] and presented in Table 4, the control surface of SIFL can always be estimated as PWL.

Table 4. Rules table based on the signed distance method

d_s	L_{NB}	L_{NM}	L_{NS}	L_{ZO}	L_{PS}	L_{PM}	L_{PB}
K_{PF}	PB	NM	NS	ZO	PS	PM	PB
K_{IF}	NB	NB	NM	ZO	PS	PM	PB
K_{DF}	PB	PM	PS	ZO	NS	NM	PB

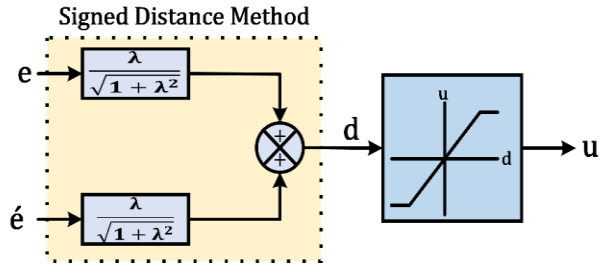

Figure. 9 SIFL with piece wise control surface

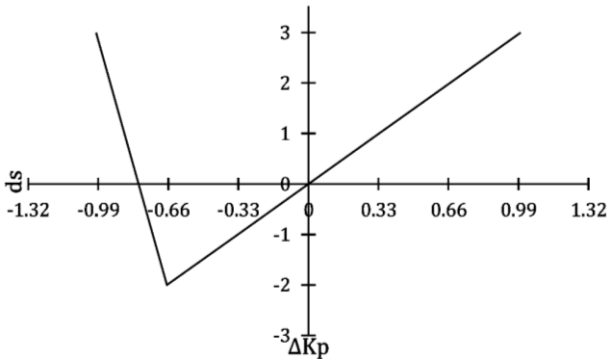

Figure. 10 The control surface of K_{pf}

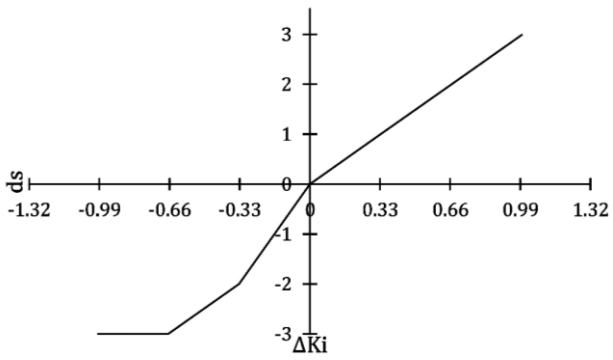

Figure. 11 The control surface of K_{if}

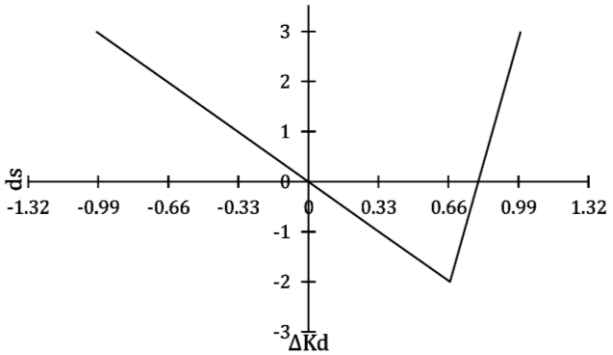

Figure. 12 The control surface of K_{df}

Table 5. Simulation parameters of two area power system

Parameter	Area 1	Area 2
Frequency of the system (Hz)	60	60
Governor speed regulation R (Hz/pu)	0.05	0.0625
Governor time constant τg (sec.)	0.2	0.3
Governor time constant τT (sec.)	0.5	0.6
Generator inertia constant H	5	4
Sensitive load frequency D (pu MW/Hz)	0.6	0.9
Frequency base factor B (pu/Hz)	20	16.92
K_p=2.8, K_i=2.4, K_d=1.5		

4. Simulation result

The two-area power system that is interconnected is designed according to the modelling system explained in Section 2 and Fig. 1. Table 5 provides the system's parameter values and their respective descriptions. Additionally, the implementation of the PID, CFL-PID, and SIFL-PID are carried out in the manner described in Section 3. The MATLAB/Simulink platform was used to run the simulations and get the results. SIFL-PID is compared with CFL-PID and PID CONTTLERS in order to evaluate its performance. Under the same system settings and variation conditions, the comparison processing is performed. The results of the simulation include the behaviours of the power system for the two-area interconnected power system when subjected to a step change in load. Hance, the load step change has been accomplished in three different scenarios.

4.1 Load disturbance in the area-1

In the first scenario, the step load change is applied on the system at t= 0 seconds with 20% of nominal power in area 1 as shown in Fig. 13 to 15. Firstly, Fig. 13 and 14 illustrate the ability of PID, CFL-PID, and SIFL-PID to attenuate the system frequency oscillations under load step changes with differences in the transient response between the three controllers.

Because of the load increase in area 1, the total load demand is already higher than the power generation that is available. Since this is the case, the frequency in areas 1 and 2 will be decreased. Secondly, Fig. 13 presents that the overshoot of the frequency deviation in area1 is considerably larger with zero overshoot of the frequency deviation in area 2, as shown in Fig. 14. This is because that the load disturbance happens in area-1 has a greater impact on the frequency in area-2. In comparison to the CFL-PID, the SIFL-PID has a low overshoot amplitude as indicate in Table 6 for the same active response and better than PID as illustrated in Fig. 13 to 15 and Table 6.

To assess the proposed method under different states, four standard formulas is used; Integral of Time-multiplied Squared Error (ITSE), Integral Time-multiplied Absolute Error (ITAE), Integral Absolute Error (IAE), and Integral Squared Error (ISE), which are given in the following equations:

$$ITSE = \int_o^{t_{sim.}} t\Delta f^2\, dt \tag{30}$$

$$ITAE = \int_o^{t_{sim.}} t|\Delta f|\, dt \tag{31}$$

$$IAE = \int_o^{t_{sim.}} |\Delta f|\, dt \tag{32}$$

$$ISE = \int_o^{t_{sim.}} \Delta f^2\, dt \tag{33}$$

From Table 7, the performance indices of the SIFL-PID are better than the FL-PID and PID

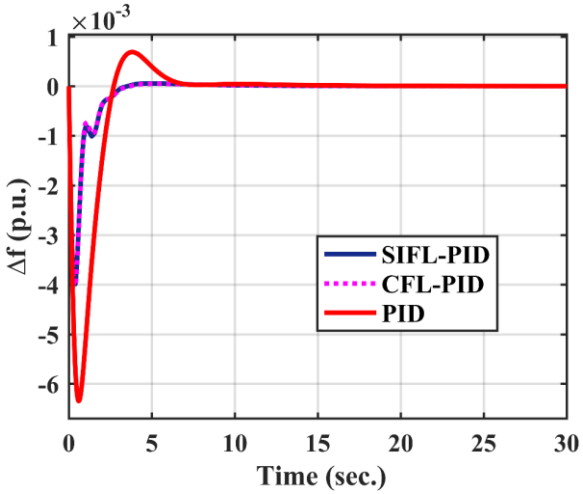

Figure. 13 Δf_1 at step change load in area 1

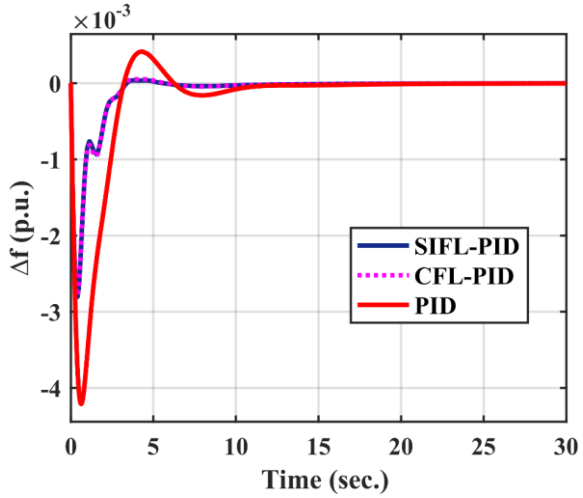

Figure. 14 Δf_2 at step change load in area 1

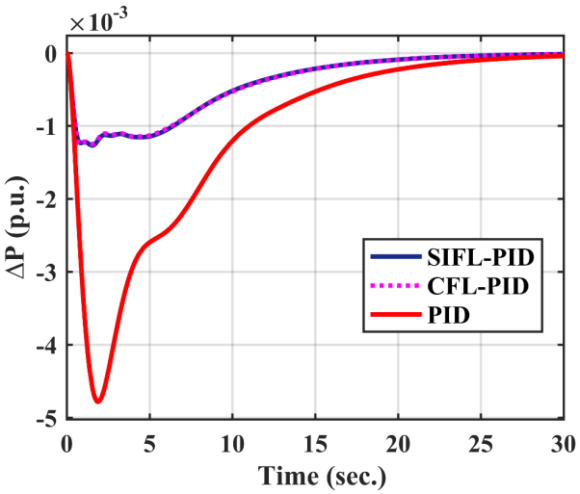

Figure. 15 ΔP_{tie} at step change load area 1

Table 6. Overshoot, undershoot, Δf and ΔP of 1st scenario

Area	Controller	PID	CFL-PID	SIFL-PID
1	overshoot	5×10^{-4}	2.1×10^{-4}	1.7×10^{-4}
	undershoot	-6.6×10^{-3}	-4.2×10^{-3}	-4.4×10^{-3}
	Δf	1.5×10^{-6}	6×10^{-7}	5.9×10^{-8}
2	overshoot	0	0	0
	undershoot	-1.2×10^{-3}	4.3×10^{-4}	4.3×10^{-4}
	Δf	-2×10^{-6}	-7.7×10^{-7}	-7.6×10^{-8}
ΔP_{tie}	overshoot	0	0	0
	undershoot	-14×10^{-3}	-6.1×10^{-3}	-5.7×10^{-3}
	ΔP	-4.2×10^{-3}	-1.6×10^{-3}	-1.6×10^{-3}

Table 7. Performance analysis standards of 1st scenario

Area	Control	PID	CFL-PID	SIFL-PID
1	ITSE	36×10^{-6}	4.2×10^{-6}	4.1×10^{-6}
	ITEA	20×10^{-3}	6.1×10^{-3}	6×10^{-3}
	IAE	11×10^{-3}	3.9×10^{-3}	3.8×10^{-3}
	ISE	4×10^{-6}	8.1×10^{-6}	8×10^{-6}
2	ITSE	20×10^{-6}	3.1×10^{-6}	3×10^{-6}
	ITEA	20×10^{-3}	6.4×10^{-3}	6.2×10^{-3}
	IAE	8×10^{-3}	3.3×10^{-3}	3.2×10^{-3}
	ISE	20×10^{-6}	4.7×10^{-6}	4.7×10^{-6}

controllers. According to these results, it can be concluded that the SIFL-PID controller is more effective.

4.2 Load disturbance in the area 2

In the second scenario, the dynamic response of the system is depicted in Fig. 16 to 18 for the same load step in section but it applied on area-2. From Fig. 16, it can be seen the good design of controllers with preferably using the SIFL-PID as indicate in Table 8.

While Fig. 18 establishes that the power flowing along the tie-line of area-1 and area-2 is positive. Because of that, the load is increased in area-2, in contract, the load in area-1 remains the same state. The power of area-1 is delivered to area-2 in order to mitigate the impact of the load increase in area-2. However, the power flow in tie line regain becomes positive value. On the other hand, the power flowing over the tie line from area-2 to area-1 is negative value, as shown in Fig. 15, because of the step-load increase in area-1 as explained in Section 2.

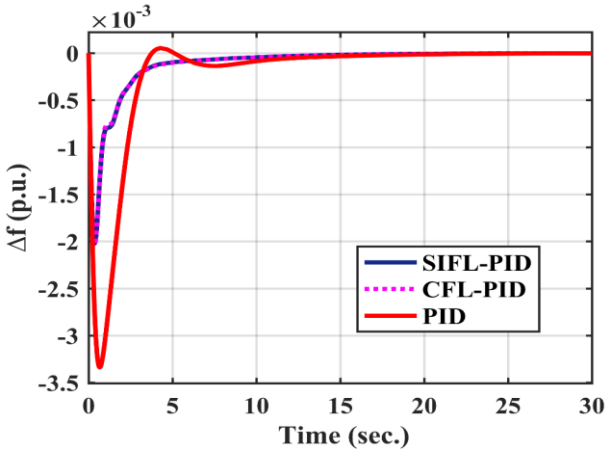

Figure. 16 Δf_1 at step change load in area 2

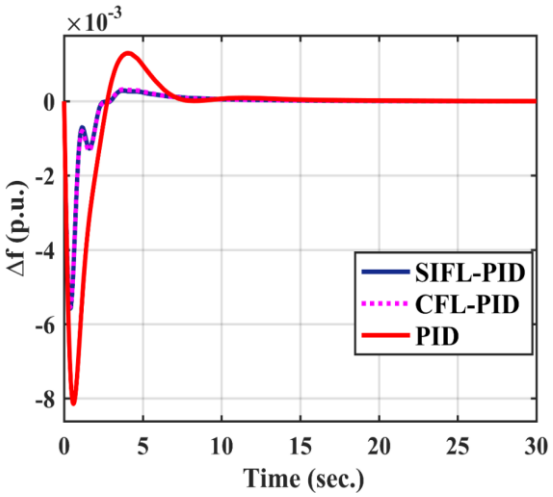

Figure. 17 Δf_2 at step change load from in area 2

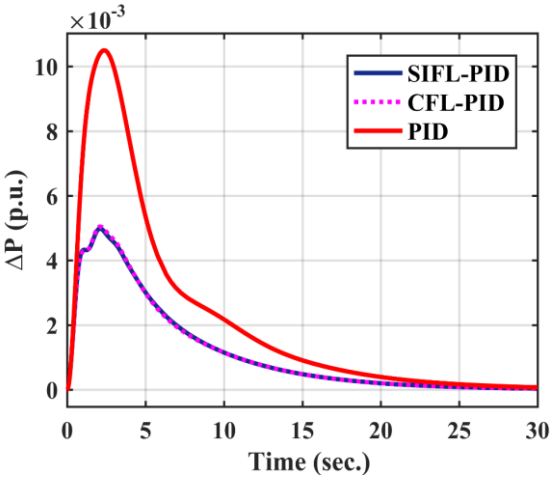

Figure. 18 ΔP_{tie} at step change load in area 2

Table 8. Performance analysis standards of 2nd scenario

Area	Control	PID	CFL-PID	SIFL-PID
1	ITSE	14×10^{-6}	2.3×10^{-6}	2.2×10^{-5}
	ITEA	20×10^{-3}	9.8×10^{-3}	9.7×10^{-3}
	IAE	7×10^{-3}	3.2×10^{-3}	3.2×10^{-3}
	ISE	14×10^{-6}	2.7×10^{-6}	2.7×10^{-6}
2	ITSE	63×10^{-6}	9.5×10^{-6}	9.3×10^{-6}
	ITEA	35×10^{-3}	14×10^{-3}	14×10^{-3}
	IAE	14×10^{-3}	6.1×10^{-3}	6×10^{-3}
	ISE	63×10^{-6}	16×10^{-6}	16×10^{-6}

4.3 Load disturbance in both areas

In the third scenario, the step load change is applied on the area-1 and the area-2 at (t= 0) seconds with (40%, and 20%) of nominal power, respectively, as shown in Fig. 19 to 21, it abundantly clears the supposed SIFL-PID superior robustness and dynamic performance irrespective of the location or magnitude of the disturbance. As compared to scenarios 1 and 2, frequency deviations in scenario 3 become larger due to higher step load changes in both areas.

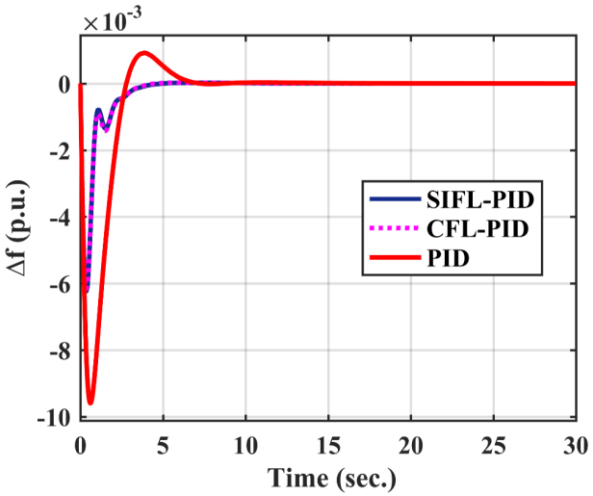

Figure. 19 Δf_1 at step change load in both areas

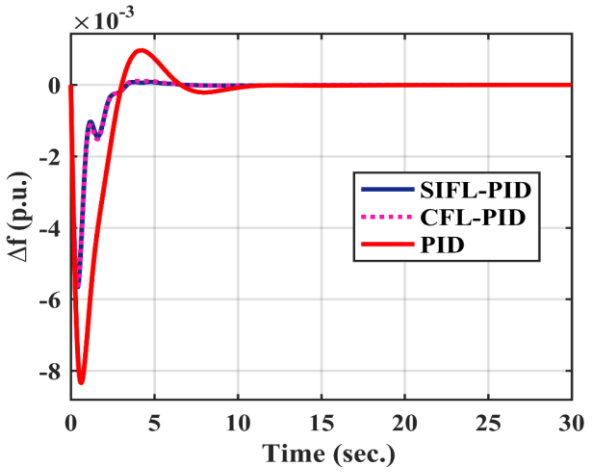

Figure. 20 Δf_2 at step change load in both areas

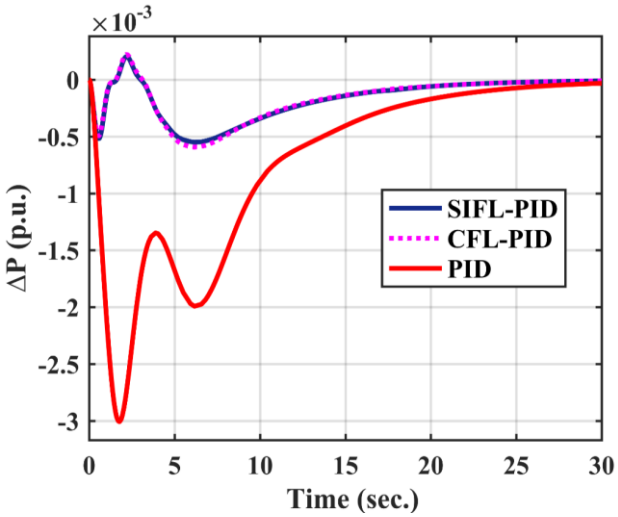

Figure. 21 ΔP_{tie} at step change load in both areas

Table 9. Performance analysis standards of 3rd scenario

Area	Control	PID	CFL-PID	SIFL-PID
1	ITSE	83×10^{-6}	9.7×10^{-6}	9.6×10^{-5}
	ITEA	25×10^{-3}	6.8×10^{-3}	6.7×10^{-3}
	IAE	16×10^{-3}	5.6×10^{-3}	5.6×10^{-3}
	ISE	9×10^{-5}	1.9×10^{-5}	1.9×10^{-5}
2	ITSE	72×10^{-6}	10×10^{-6}	9.9×10^{-6}
	ITEA	30×10^{-3}	7.6×10^{-3}	7.1×10^{-3}
	IAE	15×10^{-3}	5.7×10^{-3}	5.6×10^{-3}
	ISE	73×10^{-6}	18×10^{-6}	18×10^{-6}

5. Conclusions

In this paper, PID, FL-PID, and SIFL-PID controllers have been designed and utilized effectively to manage AGC for a two-area interconnected power system. To sum up, The PID controller's gains have been tuned by fuzzy logic algorithm. Then, the performance of controllers is validated and evaluated on a two-area power system using a MATLAB/SIMULINK. Next, the controllers' transient response performance with step-load perturbation is introduced. Based on the comparison of results, A SIFL-PID controller are clearly more efficient in terms of overshoot, undershoot, and performance standards: (ITSE), (ITAE), (IAE), and (ISE) such as in third scenario it was about 9.6×10^{-5}, 6.7×10^{-3}, 5.6×10^{-3} and $1.9\times10^{-5.}$ respectively, while, the conventional FLC method reaches to 9.7×10^{-6}, $6.8\times10^{-3,}$ 5.6×10^{-3},1.9×10^{-5} respectively, and the conventional PID reaches around; 83×10^{-6}, 25×10^{-3}, 16×10^{-3}. 9×10^{-5} respectively. Moreover, the single input fuzzy logic requires only one input with single-dimensional array for the rule table, resulting in, making its performance extremely simple to design, implementation, and good for the tuning process.

Conflicts of Interest

The authors declare no conflict of interest.

Author Contributions

S.D.A.-M., M.K.A.-N. and A.J.M. are the main authors who conducted the system design and simulations. A.M.D., M.F.A. and H.S.A.-R. supervised the work and contributed to the editing of the document. All authors have read and agreed to the published version of the manuscript.

Acknowledgments

The authors would like to express their thanks to our colleagues in the Department of Electrical Engineering in the College of Engineering at Misan University for their unconditional support during the duration of this work.

References

[1] Y. Arya, "A new optimized fuzzy FOPI-FOPD controller for automatic generation control of electric power systems", *Journal of The Franklin Institute*, Vol. 356, No. 11, pp. 5611-5629, 2019.

[2] K. Ullah, A. Basit, Z. Ullah, S. Aslam, and H. Herodotou, "Automatic generation control strategies in conventional and modern power systems: A comprehensive overview", *Energies*, Vol. 14, No. 9, p. 2376, 2021.

[3] H. Bevrani and T. Hiyama, "Intelligent Automatic Generation Control.", *CRC Press*, 2011.

[4] Y. Arya, "Improvement in automatic generation control of two-area electric power systems via a new fuzzy aided optimal PIDN-FOI controller", *ISA Transactions*, Vol. 80, pp. 475-490, 2018.

[5] A. G. Marzbali, "Multi-area multi-source automatic generation control in deregulated power system", *Energy*, Vol. 201, p. 117667, 2020.

[6] A. Aziz, G. Shafiullah, A. M. T. Oo, and A. Stojcevski, "Automatic generation control in wind integrated power system: new perspectives and challenges", *International Journal of Thermal Environmental Engineering*, Vol. 12, No. 1, pp. 27-38, 2016.

[7] Y. Arya, "Automatic generation control of two-area electrical power systems via optimal fuzzy classical controller", *Journal of The Franklin Institute*, Vol. 355, No. 5, pp. 2662-2688, 2018.

[8] P. A. Gbadega and K. T. Akindeji, "Linear quadratic regulator technique for optimal load frequency controller design of interconnected linear power systems", In: *Proc. of 2020 IEEE PES/IAS PowerAfrica*, pp. 1-5, 2020.

[9] M. I. Alomoush, "Load frequency control and automatic generation control using fractional-order controllers", *Electrical Engineering*, Vol. 91, No. 7, pp. 357-368, 2010.

[10] P. McNamara and F. Milano, "Model predictive control-based AGC for multi-terminal HVDC-connected AC grids", *IEEE Transactions on Power Systems*, Vol. 33, No. 1, pp. 1036-1048, 2017.

[11] M. K. Sarkar, A. Dev, P. Asthana, and D. Narzary, "Chattering free robust adaptive integral higher order sliding mode control for load frequency problems in multi‐area power systems", *IET Control Theory & Applications*, Vol. 12, No. 9, pp. 1216-1227, 2018.

[12] M. K. A. Nussairi and R. Bayindir, "Co-simulation of Fuzzy Logic Control for a DC–DC Buck Converter in Cascade System", In: *Proc. of Artificial Intelligence and Evolutionary Computations in Engineering Systems*, pp. 561-569, 2020.

[13] S. S. Pati, S. Dash, and S. K. Mishra, "Performance Comparison of Fuzzy Gain Scheduling based LFC Controller in Deregulated AGC of a Multi Area System Incorporating Wind Energy", In: *Proc. of International Conf. on Applied Electromagnetics*, pp. 1-6, 2018.

[14] L. Keltoum, B. Leila, and B. Abderrahmen, "Speed control of a Doubly-Fed induction motor (DFIM) based on fuzzy sliding mode controller", *International Journal of Intelligent Engineering Systems*, Vol. 10, No. 3, pp. 20-29, 2017.

[15] M. K. A. Nussairi and R. Bayindir, "Stabilization of a DC-Link of Microgrids feeding a Inverter-BLDC motor drive using a PI-Fuzzy", In: *Proc. of 7th International Conf. on Renewable Energy Research and Applications*, pp. 1514-1519, 2018.

[16] N. Baharudin and S. Ayob, "Brushless DC motor drive control using single input fuzzy PI controller (SIFPIC)", In: *Proc. of IEEE Conf. on Energy Conversion*, pp. 13-18, 2015.

[17] K. V. Chandrakala, S. Balamurugan, and K. Sankaranarayanan, "Variable structure fuzzy gain scheduling based load frequency controller for multi source multi area hydro thermal system", *International of Electrical Power & Energy Systems*, Vol. 53, pp. 375-381, 2013.

[18] F. N. Zohedi, M. S. M. Aras, H. A. Kasdirin, and N. B. Nordin, "New lambda tuning approach of single input fuzzy logic using gradient descent algorithm and particle swarm optimization",

Indonesian Journal of Electrical Engineering Computer Science, Vol. 25, No. 3, pp. 1344-1355, 2022.

[19] M. Mokhtari, S. Zouggar, N. K. M'sirdi, and M. L. Elhafyani, "Voltage regulation of an asynchronous wind turbine using STATCOM and a control strategy based on a combination of single input fuzzy logic regulator and sliding mode controllers", *International Journal of Power Electronics Drive Systems*, Vol. 11, No. 3, p. 1557, 2020.

[20] O. Saleem, U. T. Shami, and K. M. Hasan, "Time optimal control of DC – DC buck converter using single input fuzzy augmented fractional order PI controller", *International Transactions on Electrical Energy Systems*, Vol. 29, No. 10, pp. 1-20, 2019.

[21] G. V. Lakhekar, L. M. Waghmare, and R. G. Roy, "Disturbance observer-based fuzzy adapted S-surface controller for spatial trajectory tracking of autonomous underwater vehicle", *IEEE Transactions on Intelligent Vehicles*, Vol. 4, No. 4, pp. 622-636, 2019.

[22] B. J. Choi, S. W. Kwak, and B. K. Kim, "Design and stability analysis of single-input fuzzy logic controller", *IEEE Transactions on Systems, Man, Cybernetics, Part B*, Vol. 30, No. 2, pp. 303-309, 2000.

[23] Y. Yuan, C. Chang, Z. Zhou, X. Huang, and Y. Xu, "Design of a single-input fuzzy PID controller based on genetic optimization scheme for DC-DC buck converter", In: *Proc. of International Symposium on Next-Generation Electronics*, pp. 1-4, 2015.

[24] D. Suresh and S. P. Singh, "Design of single input fuzzy logic controller for shunt active power filter", *IETE Journal of Research*, Vol. 61, No. 5, pp. 500-509, 2015.

[25] M. K. A. Nussairi, S. D. A. Majidi, A. R. Hussein, and R. Bayindir, "Design of a Load Frequency Control based on a Fuzzy logic for Single Area Networks", In: *Proc. of International Conf. on Renewable Energy Research and Application*, pp. 216-220, 2021.

[26] M. Mokhtari, S. Zouggar, M. L. Elhafyani, T. Ouchbel, N. K. M'sirdi, and A. Naaman, "Voltage stability improvement of an asynchronous wind turbine using static var compensator with single input fuzzy logic controller", In: *Proc. of 6th Int. Renewable and Sustainable Energy Conf*, pp. 1-6, 2018.

[27] S. D. A. Majidi, M. K. A. Nussairi, A. J. Mohammed, A. M. Dakhil, M. F. Abbod, and H. S. A. Raweshidy, "Design of a Load Frequency Control based on a Optimal neural Network", *Energies*, Vol. 15, No. 17, p. 6223, 2022.

Notations

$\Omega(s)$	The speed of the synchronous-generator
H	The inertia of the synchronous generator
ΔP_m	mechanical power deviation
ΔP_e	electrical power deviation
e_1, e_2	Area control errors
Δe	Change of Area control errors
B_1, B_2	Frequency base factors
ΔP_{ref1}, ΔP_{ref2}	Power reference deviations
ΔP_{v1}, ΔP_{v2}	Governor valve position deviations
$\boldsymbol{\tau}_{g1}$, $\boldsymbol{\tau}_{g2}$	Governor time constants
ΔP_{g1}, ΔP_{g2}	Output power deviation of Governor
$\boldsymbol{\tau}_{T1}$, $\boldsymbol{\tau}_{T2}$	Turbine time constants
ΔP_{T1}, ΔP_{T2}	Output power deviation of Turbine
ΔP_1, ΔP_2	Load disturbance s
K_1, K_2	Constants of power system
$\boldsymbol{\tau}_{p}1$, $\boldsymbol{\tau}_{p2}$	Power system time constants
Δf_1, Δf_2	Frequency deviations
ΔP_L	the changes of a resistive load
D	Sensitive factor of Frequency deviations
$\Delta\omega$	speed deviation of the synchronous-generator
R_1, R_2	The speed regulators of governor
ΔP_{tie}	Tie-line power deviation
E_1, E_2	Voltage of generators
δ_1, δ_2	Rotor angles
X_1,X_2,X_{12}	Reactance of area 1, 2 and tie line
α	Synchronizing Coefficient for Tie Line